scientific reports

Check for updates

OPEN

Exploring strong and weak topological states on isostructural substitutions in $TlBiSe_2$

Ankita Phutela✉, Preeti Bhumla, Manjari Jain & Saswata Bhattacharya✉

Topological Insulators (TIs) are unique materials where insulating bulk hosts linearly dispersing surface states protected by the Time-Reversal Symmetry. These states lead to dissipationless current flow, which makes this class of materials highly promising for spintronic applications. Here, we predict TIs by employing state-of-the-art first-principles based methodologies, viz., density functional theory and many-body perturbation theory (G_0W_0) combined with spin-orbit coupling effects. For this, we take a well-known 3D TI, $TlBiSe_2$ and perform complete substitution with suitable materials at different sites to check if the obtained isostructural materials exhibit topological properties. Subsequently, we scan these materials based on SOC-induced parity inversion at Time-Reversal Invariant Momenta. Later, to confirm the topological nature of selected materials, we plot their surface states along with calculation of Z_2 invariants. Our results show that $GaBiSe_2$ is a strong Topological Insulator, besides, we report six weak Topological Insulators, viz., $PbBiSe_2$, $SnBiSe_2$, $SbBiSe_2$, Bi_2Se_2, $TlSnSe_2$ and $PbSbSe_2$. We have further verified that all the reported TIs are dynamically stable, showing all real phonon modes of vibration.

Since the discovery of Topological Insulators (TIs) about a decade ago, there has been an enormous increase in interest towards topological condensed matter systems[1–13]. TIs show great potential applications in quantum computing and spintronics due to the insensitivity of the transport property towards non-magnetic perturbations[13,14]. TIs also pave the way for realizing advanced quantum phenomena such as Weyl semimetals[15], Majorana-fermions[16] and Higgs mechanism[17]. These alluring materials are insulating in bulk but support the flow of electrons on their surface. As a result, their surface consists of linear states that are protected by the Time-Reversal Symmetry (TRS)[18]. A necessary condition for the appearance of these states is the inversion of bands, which takes place at the Time-Reversal Invariant Momenta (TRIM) in the bulk Brillouin Zone (BZ)[19,20]. The natural ordering of the energy levels forming the edges of the gap is inverted owing to the strong Spin-Orbit Coupling (SOC) associated with heavy elements. The topology of TRS invariant insulators is characterized by the Z_2 index, ν_0, which can either be 0 or 1, depicting a topologically trivial or non-trivial phase, respectively. However, it has been recently reported that even when $\nu_0 = 0$, the system can show non-trivial characteristics[21]. Based on whether the material hosts odd or even number of Dirac cones in the electronic structure of its surface, TIs are further classified as Strong Topological Insulator (STI) having Z_2 invariant, $\nu_0 = 1$ or Weak Topological Insulator (WTI) with Z_2 invariant, $\nu_0 = 0$[22,23]. Nevertheless, the complete characterization of 3D TIs requires a set of, in total, four Z_2 numbers: (ν_0;$\nu_1\,\nu_2\,\nu_3$). The indices ν_1, ν_2 and ν_3 are called weak indices and are believed to be nonrobust quantities[24,25]. Therefore, the calculation of surface states and Z_2 invariant gives complete information about the topological nature of material.

First-principles calculations led to the prediction of a large number of 2D and 3D TIs[22,26–34]. Among the various well established families of 3D TIs, Bi_2Se_3 and Bi_2Te_3 have been most widely studied for investigating the topological states and their properties[35–37]. Their crystal structures consist of quintuple layers held together by weak van der Waals (vdW) forces, providing natural cleavage planes without breaking strong bonds. The band structure calculations in Bi_2Se_3 have shown that the Dirac point of surface state lies close to the Valence Band Maximum (VBM)[38]. This leads to the opening of electron scattering channel from surface states to bulk continuum states, and the topological transport regime begins to collapse. Therefore, there is a strong need for materials with ideal and relatively isolated Dirac cones. A variety of candidates with non-trivial electronic states including, HgTe[39], InAs[40], ternary tetramytes $Ge_mBi_{2n}Te_{(m+3n)}$, half-Huesler compounds[41,42], LiAuSe honeycomb lattice[43], β-Ag_2Te[44] to non-centrosymmetric BiTeX (X=Cl, Br, I)[45] have been suggested. Theoretical studies have shown that Tl-based ternary chalcogenides, viz., $TlSbTe_2$, $TlBiSe_2$ and $TlBiTe_2$ are 3D TIs with a single Dirac

Department of Physics, Indian Institute of Technology Delhi, New Delhi 110016, India. ✉email: ankita@physics.iitd.ac.in; saswata@physics.iitd.ac.in

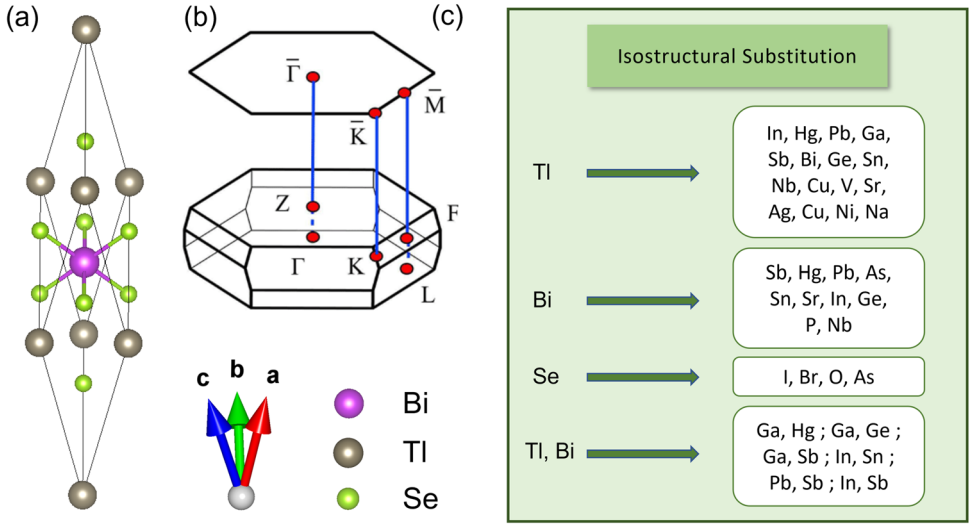

Figure 1. (**a**) Primitive crystal structure of $TlBiSe_2$, (**b**) 3D BZ for primitive unit cell with four time-reversal invariant points Γ, Z, F and L along with the projected surface BZ, and (**c**) complete substitution with various elements at Tl, Bi, Se and Tl, Bi sites simultaneously.

cone surface state at the Γ point, which is well isolated from the bulk continuum[46]. Tl-based materials have a 3D character because each Tl (Bi) layer is sandwiched between two Se layers with strong coupling between neighboring atomic layers instead of weak vdW forces as in Bi_2Se_3. The electronic structure of many Tl-based TIs, viz., $TlAB_2$ (A = Sb, Bi and B = Se, Te, S) have been investigated by Density Functional Theory (DFT) calculations[20,47]. The role of surface termination has also been explored in $TlBiSe_2$ and $TlBiTe_2$[48]. Following this, the isostructural substitution of the above base material is been endeavoured to retain its topological properties. For example, In-based compounds like $InBiTe_2$ and $InSbTe_2$, crystallizing in the $TlBiSe_2$ like crystal structure have been studied. Intriguingly, these materials lack the Dirac cone feature, which depicts their topologically trivial nature[49]. Therefore, despite $TlAB_2$ (A = Sb, Bi and B = Se, Te, S) showing topologically non-trivial band structure, any other isostructural substitution to retain its topological nature is hitherto unknown.

Motivated with this idea, in this article, we have explored the possibility of having materials belonging to same class of ternary chalcogenides via a thorough isostructural substitution approach. First, we have performed substitution at suitable sites of $TlBiSe_2$ and scanned for those materials whose band structure shows band inversion at odd/even number of TRIMs. After that, to determine the accurate band gap of $TlBiSe_2$, we have employed various exchange-correlation (ϵ_{xc}) functionals, viz., PBE+SOC, HSE06+SOC, G_0W_0@PBE+SOC and G_0W_0@HSE06+SOC. The band gap obtained from G_0W_0@PBE+SOC functional is in close agreement with the experimental value. Therefore, we have further calculated the band gap of all materials using G_0W_0@PBE+SOC. Subsequently, we have examined the potential materials for their dynamical stability. The stable materials are then characterized as STI/WTI depending on whether they show odd/even number of surface states, respectively. To confirm their topological nature, we have also calculated the Z_2 topological invariants.

Results and discussion

Bulk electronic structure and band inversion. $TlBiSe_2$ belongs to the Tl-family of compounds having a rhombohedral crystal structure with space group $R\bar{3}m$[46]. There are four atoms in the primitive unit cell which are placed in layers normal to the three-fold axis with the sequence -Tl-Se-Bi-Se-, i.e., along [111] axis of rhombohedral unit cell (see Fig. 1a). The 3D BZ for rhombohedral unit cell having high symmetry points F, Γ, L and Z, along with its projected (111) surface BZ is shown in Fig. 1b. The structure has inversion symmetry where both Bi and Tl act as inversion centers. We have first estimated the band gap of $TlBiSe_2$ using PBE+SOC functional. The calculated band gap is 215 meV (direct), whereas the experimental band gap is 350 meV[50]. The band gap is thus underestimated due to the DFT limitation arising from the approximations used in the ϵ_{xc} functional. Therefore, we have used hybrid ϵ_{xc} functional (HSE06) with default $\alpha = 0.25$, i.e., incorporating 25% of Hartree-Fock exact exchange to capture the electron's self-interaction error along with SOC. It gives a direct band gap of 85 meV, which is also not in accordance with previously reported theoretical calculations[48]. Therefore, we have performed G_0W_0 calculations on top of the orbitals obtained from the PBE+SOC (G_0W_0@PBE+SOC) and HSE06+SOC (G_0W_0@HSE06+SOC) ϵ_{xc} functional. The respective band gaps are 280 meV and 249 meV (see Table 1). G_0W_0@PBE+SOC gives the most accurate band gap, however, the band profile is not much affected by the choice of ϵ_{xc} functional (see Section I of Supplementary Information). Therefore, we have used PBE ϵ_{xc} functional to plot the band structures in view of its low computational cost. The band structure of $TlBiSe_2$ with the projected wavefunctions to atomic orbitals is shown in Fig. 2a. The Conduction Band (CB) is dominated by Bi-*p* and Tl-*p* orbitals, while Se-*p* orbitals dominate the Valence Band (VB). The inclusion of SOC has led to an increase in the band gap around the Γ point. The valence and conduction band edges switch their

PBE+SOC (meV)	HSE06+SOC (meV)	G_0W_0@PBE+SOC (meV)	G_0W_0@ HSE06+SOC (meV)
215	85	280	249

Table 1. Band gap of $TlBiSe_2$ using different ϵ_{xc} functionals.

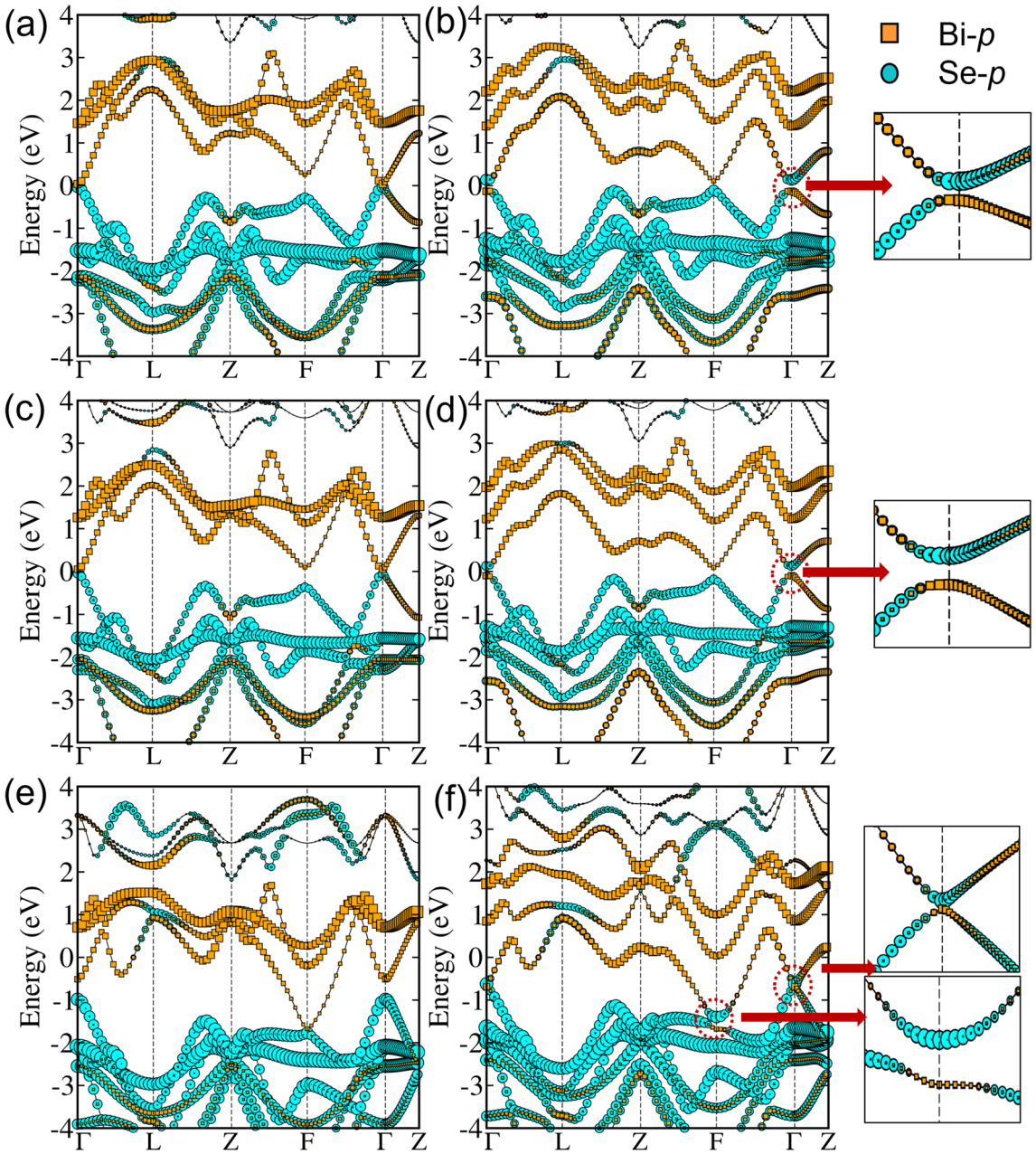

Figure 2. The band structures for $TlBiSe_2$, $GaBiSe_2$ and $PbBiSe_2$ without SOC are shown in (**a**), (**c**), (**e**) and with SOC are shown in (**b**), (**d**), (**f**), respectively. Insets show band inversion at respective high symmetry points.

orbital character around this point, indicating the band inversion. The *p* orbitals of Se and Bi are involved in this band inversion, as can be clearly seen from Fig. 2b.

The similar band inversion has also been observed in $TlBiTe_2$ and $TlSbSe_2$[48]. Following the trend, we have carried out complete substitution in $TlBiSe_2$ at Tl, Bi or Se sites and Tl, Bi sites simultaneously to obtain different materials belonging to the same class (see Fig. 1c). The band structures of these materials are plotted to see the effect of SOC on the orbital contribution projected on the bands lying near Fermi level. Firstly, Ga is substituted at the Tl site (Ga_{Tl}) to form $GaBiSe_2$. It also crystallizes in $R\bar{3}m$ phase with lattice parameters given as $a = b = c = 7.18$ Å (in rhombohedral setting) and yields the band structure shown in Fig. 2c. SOC driven inversion of energy levels along with opening of band gap takes place at high symmetry point Γ (Fig. 2d). The

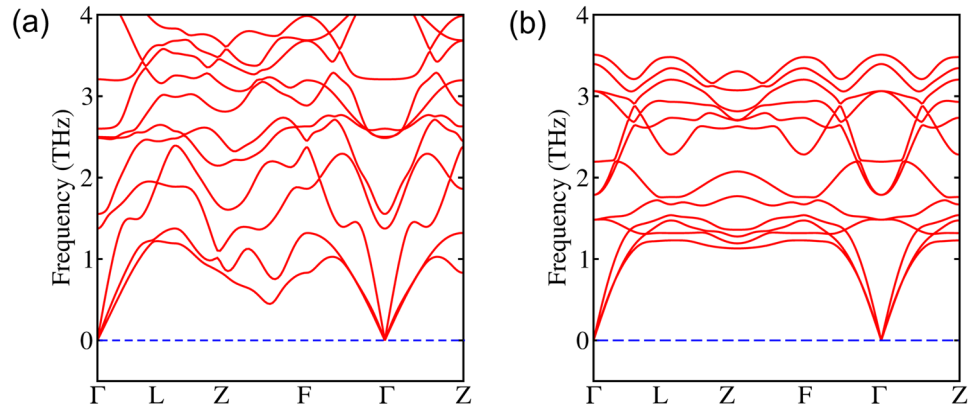

Figure 3. Phonon band structures of (**a**) $GaBiSe_2$ and (**b**) $PbBiSe_2$.

Material	Indirect band gap (meV)
$GaBiSe_2$	183
$PbBiSe_2$	3
$SnBiSe_2$	20
$SbBiSe_2$	118
Bi_2Se_2	327
$TlSnSe_2$	44
$PbSbSe_2$	41

Table 2. Band gap of different materials using G_0W_0@PBE+SOC.

projected wavefunctions to atomic orbitals show that *p* orbitals of all atoms contribute near the Fermi level. The inversion involves Bi-*p* and Se-*p* orbitals (for details see Section II of Supplementary Information), giving an initial indication that the material can harbor non-trivial topological phase. The indirect band gap as calculated by G_0W_0@PBE+SOC is 183 meV.

After $GaBiSe_2$, we have substituted Pb_{Tl} to get $PbBiSe_2$ having lattice parameters as $a = b = c = 8.27$ Å, and crystallizing in the $R\bar{3}m$ phase. G_0W_0@PBE+SOC yields an indirect band gap of 3 meV. The VB and CB are mainly composed of *p* orbitals of Pb, Bi and Se, as shown in Fig. 2e and f. The parity inversion occurs at Γ and F points, unlike the former. In this BZ, there are 8 TRIMs, i.e., Γ, Z (non-degenerate) and F, L (triply-degenerate). Therefore, the inversion is occurring at even number of TRIMs, which means that the system should be in trivial state. However, it has been found that if even number of band inversions occur in the first quadrant, but if one or more BZ sides possess odd number of band inversions, then a WTI can be obtained[31].

A similar type of parity inversion at even number of TRIMs is obtained for $SnBiSe_2$, $SbBiSe_2$, Bi_2Se_2, $TlSnSe_2$ and $PbSbSe_2$ (refer Section III and Section IV of Supplementary Information for band structures and optimized lattice parameters, respectively). The band gaps of all these materials calculated using G_0W_0@PBE+SOC are given in Table 2. After screening the systems for SOC-induced inversion in the band structures, we have analyzed them for dynamical stability. Figure 3 shows the phonon band structures for $GaBiSe_2$ and $PbBiSe_2$. The absence of negative frequencies confirms the dynamical stability of these materials. For other systems showing band inversion, the dynamical stability is given in Section V of Supplementary Information.

Topological surface states and Z_2 invariant. The presence of band inversion on inclusion of SOC is a telltale signature of possibility of non-trivial phase. However, an inverted band structure cannot be considered as a sole criterion to assure the existence of a non-trivial phase. Therefore, further analysis is required to establish its topological nature. Previous studies have reported that non-trivial band topology generates metallic surface states, which are the hallmark of TIs[51]. In view of this, we have computed the spectrum of surface states by considering a semi infinite slab of 3D material. These lattice surfaces possess Dirac cones, lying at the same *k*-point where the band inversion has occurred in the corresponding bulk band structure. Furthermore, to elucidate the topological nature of the materials, Z_2 topological invariants are calculated. TRS yields four distinct Z_2 invariants ($\nu_0;\nu_1\nu_2\nu_3$) in 3D case. Each of these four invariants takes up value either 0 or 1, indicating a total of 16 phases with three general classes: a normal insulator, an STI and a WTI[25]. An ordinary or trivial insulator is obtained when all four invariants are zero, i.e., (0;000), while an STI is obtained when $\nu_0 = 1$. This type of system is robust against weak time-reversal invariant perturbations. However, when $\nu_0 = 0$, and at least one of the indices out of ν_1, ν_2 or ν_3 is nonzero, then the material is WTI. It can be viewed as a stacking of 2D TIs, and is less robust against perturbations.

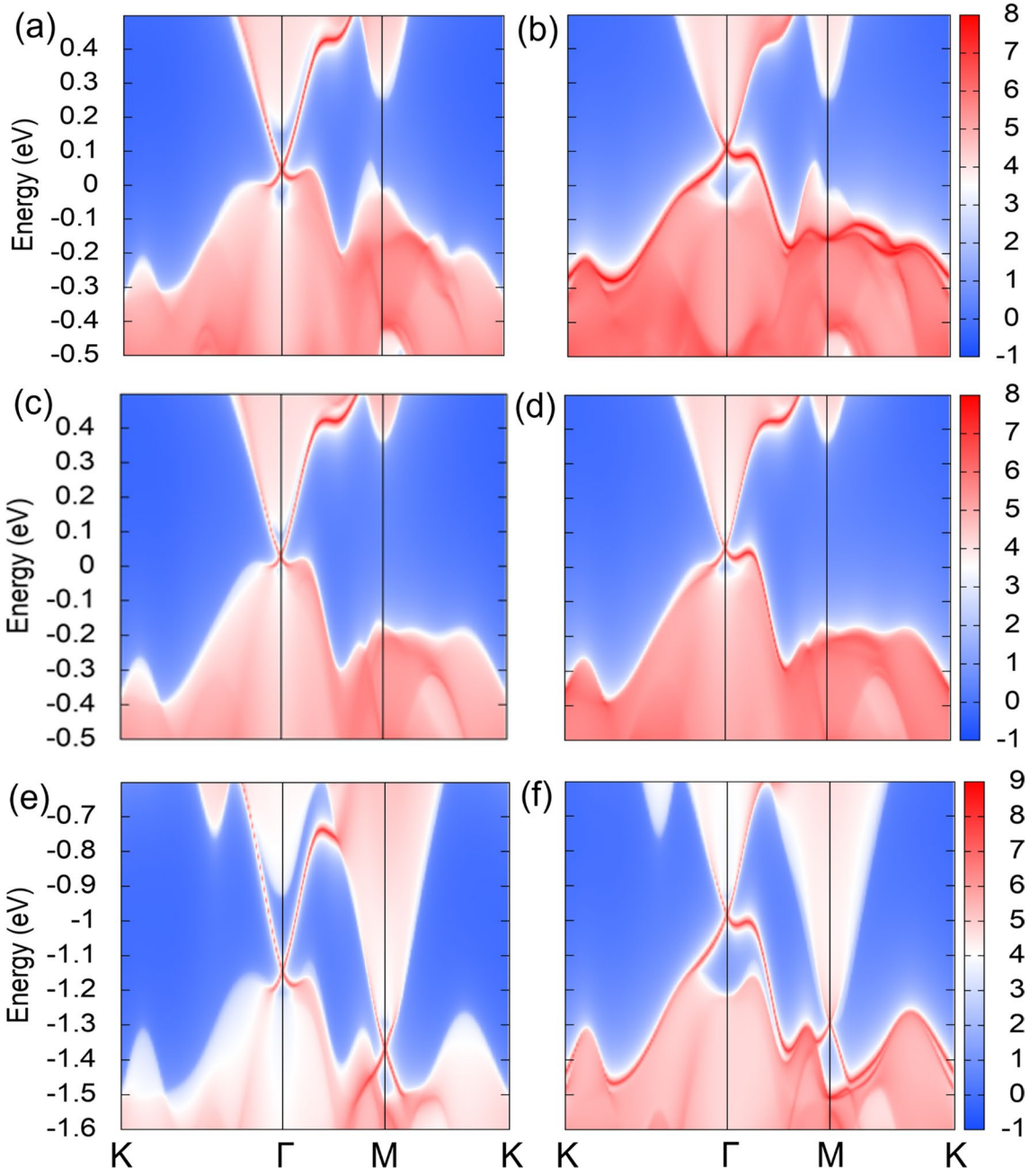

Figure 4. Surface states for the left surface of $TlBiSe_2$, $GaBiSe_2$ and $PbBiSe_2$ are shown in (**a**), (**c**), (**e**) and for the right surface are shown in (**b**), (**d**), (**f**), respectively. Here, the sharp red curves represent surface states, whereas, the shaded regions show the spectral weight of projected bulk bands.

It has already been established that $TlBiSe_2$ is a strong 3D TI[52]. On that account, we first obtain its surface band structure. For this, a tight-binding Hamiltonian with MLWFs considering the projection of *p* orbitals of Bi/Se and *sp* orbitals of Tl is constructed. Since the left and right surface for $TlBiSe_2$ terminates with different atoms (Tl and Se, respectively), therefore, we have plotted surface state spectra of (111) surface for both the surface terminations. Figure 4a and b show a single surface state protected by TRS at the Γ point in the projected 2D BZ. Alongside, we have calculated the topological invariant, ν_0, which comes out to be 1, confirming that $TlBiSe_2$ is an STI. Following this, we have explored $GaBiSe_2$ for topological properties. In this case, the *p* orbitals of Bi/Se and *sp* orbitals of Ga are considered in constructing the tight-binding Hamiltonian. A single Dirac cone protected by TRS has been observed for (111) surface (see Fig. 4c and d), and the corresponding topological invariant is (1;000), which is a signature of non-trivial topology. This validates that $GaBiSe_2$ is an STI.

Afterwards, we have performed surface band structure calculation for $PbBiSe_2$. We have obtained even (two) number of surface states lying at Γ and M along (111) direction (see Fig. 4e and f). The presence of even number of surface states yields $\nu_0 = 0$, and the weak indices come out to be $\nu_1 = 0$, $\nu_2 = 0$ and $\nu_3 = 1$. As even number of surface states lead to scattering and are not topologically protected, hence this material is categorized as a WTI.

Material	$Z_2:(\nu_0;\nu_1\nu_2\nu_3)$	Number of surface states	Type
$GaBiSe_2$	(1;000)	1	STI
$PbBiSe_2$	(0;001)	2	WTI
$SnBiSe_2$	(0;001)	2	WTI
$SbBiSe_2$	(0;001)	2	WTI
Bi_2Se_2	(0;001)	2	WTI
$TlSnSe_2$	(0;001)	2	WTI
$PbSbSe_2$	(0;111)	2	WTI

Table 3. Calculated Z_2 invariants for different materials.

The similar calculations are performed for $SnBiSe_2$, $SbBiSe_2$, Bi_2Se_2, $TlSnSe_2$ and $PbSbSe_2$. All of them show even number of surface states along (111) direction, as shown in Section VI of Supplementary Information, and corresponding Z_2 invariants are given in Table 3. These materials belong to the class of Z_2 WTI. Nowadays, WTIs are also getting attention as it has been found that their surface states are robust against imperfections, owing to the delocalization of surface electrons[53].

Conclusions

In summary, we have performed isostructural substitution of materials based on SOC-induced parity inversion in the band structure. Using first-principles based methodologies, viz., PBE, HSE06, and many-body perturbation theory (G_0W_0), we have systematically studied the electronic structure of topological materials belonging to $R\bar{3}m$ space group. The band gap calculated using G_0W_0@PBE+SOC is in close agreement with the experimental value. We have confirmed that $GaBiSe_2$ is an STI as its surface accommodates a single crossing at the Γ point. $PbBiSe_2$, $SnBiSe_2$, $SbBiSe_2$, Bi_2Se_2, $TlSnSe_2$ and $PbSbSe_2$ are WTI catering even number of surface states within the bulk band gap. The absence of negative frequencies in the phonon band structures indicates dynamical stability. The calculated Z_2 invariants are in accordance with the surface state plots confirming their topological nature. We believe, exploring these materials both theoretically and experimentally will offer a great platform for studying intriguing quantum effects.

Methods

The calculations are performed using DFT[54,55] with the Projected Augmented Wave (PAW)[56,57] method implemented in Vienna *Ab initio* Simulation Package (VASP)[58] code. All the structures are optimized with the Generalized Gradient Approximation (GGA) of Perdew-Burke-Ernzerhof (PBE)[59] until the Hellmann-Feynman forces are smaller than 0.001 eV/Å. The plane wave basis is used with 400 eV cutoff energy. The Γ-centered 6×6×4 *k*-grid is used to sample the irreducible BZ of rhombohedral phase with the $R\bar{3}m$ space group. SOC is included in all calculations except in ionic optimization. The advanced hybrid ϵ_{xc} functional (HSE06) including SOC and many-body perturbation methods, G_0W_0@PBE+SOC and G_0W_0@HSE06+SOC are used for the better estimation of the band gap[60]. For this, we have used 4×4×4 *k*-grid, and the number of bands is set to six times the number of occupied bands. The phonon calculations are performed with 4×4×4 supercells using the PHONOPY package[61,62]. In order to investigate the topological properties of the materials, we have performed DFT calculations using fully relativistic norm-conserving pseudopotentials as implemented in the QUANTUM ESPRESSO code[63]. The results of these DFT calculations are then fed as input to WANNIER90[64] for constructing a tight-binding model based on Maximally Localized Wannier Functions (MLWFs) with *p* orbitals of Se, Bi and *sp* orbitals of Ga, Tl, Sn, Sb, Pb. The surface states and topological invariants are then calculated using the Green's function method as implemented in the Wannier-TOOLS package[65].

Data availibility

The data that support the findings of this study are available from the corresponding author upon reasonable request.

Received: 26 July 2022; Accepted: 14 December 2022
Published online: 20 December 2022

References

1. Fan, Z., Liang, Q.-F., Chen, Y., Yao, S.-H. & Zhou, J. Transition between strong and weak topological insulator in $ZrTe_5$ and $HfTe_5$. *Sci. Rep.* **7**, 1–7 (2017).
2. Feng, L.-Y. *et al.* Prediction of topological Dirac semimetal in Ca-based Zintl layered compounds CaM_2X_2 (M= Zn or Cd; X= N, P, As, Sb, or Bi). *Sci. Rep.* **12**, 1–8 (2022).
3. Moore, J. E. The birth of topological insulators. *Nature* **464**, 194–198 (2010).
4. Fu, L., Kane, C. L. & Mele, E. J. Topological insulators in three dimensions. *Phys. Rev. Lett.* **98**, 106803 (2007).
5. Niu, C. *et al.* Realization of tunable Dirac cone and insulating bulk states in topological insulators $(Bi_{(1-x)}Sb_x)_2Te_3$. *Sci. Rep.* **2**, 1–7 (2012).
6. Kou, L. *et al.* Robust 2d topological insulators in van der waals heterostructures. *ACS Nano* **8**, 10448–10454 (2014).
7. Ma, Y., Dai, Y., Kou, L., Frauenheim, T. & Heine, T. Robust two-dimensional topological insulators in methyl-functionalized bismuth, antimony, and lead bilayer films. *Nano Lett.* **15**, 1083–1089 (2015).

8. Chen, Y. *et al.* High-pressure phase transitions and structures of topological insulator BiTeI. *J. Phys. Chem. C* **117**, 25677–25683 (2013).
9. Qi, X. L., Hughes, T. L. & Zhang, S. C. Topological field theory of time-reversal invariant insulators. *Phys. Rev. B* **78**, 195424 (2008).
10. Moore, J. E. & Balents, L. Topological invariants of time-reversal-invariant band structures. *Phys. Rev. B* **75**, 121306 (2007).
11. Hasan, M. Z. & Kane, C. L. Colloquium: Topological insulators. *Rev. Mod. Phys.* **82**, 3045 (2010).
12. Chiu, C. K., Teo, J. C., Schnyder, A. P. & Ryu, S. Classification of topological quantum matter with symmetries. *Rev. Mod. Phys.* **88**, 035005 (2016).
13. Qi, X. L. & Zhang, S. C. Topological insulators and superconductors. *Rev. Mod. Phys.* **83**, 1057 (2011).
14. Wan, X., Turner, A. M., Vishwanath, A. & Savrasov, S. Y. Topological semimetal and fermi-arc surface states in the electronic structure of pyrochlore iridates. *Phys. Rev. B* **83**, 205101 (2011).
15. Singh, B. *et al.* Topological electronic structure and weyl semimetal in the $TlBiSe_2$ class of semiconductors. *Phys. Rev. B* **86**, 115208 (2012).
16. Wilczek, F. Majorana returns. *Nat. Phys.* **5**, 614–618 (2009).
17. Sato, T. *et al.* Unexpected mass acquisition of dirac fermions at the quantum phase transition of a topological insulator. *Nat. Phys.* **7**, 840–844 (2011).
18. Kane, C. L. & Mele, E. J. Z_2 topological order and the quantum spin hall effect. *Phys. Rev. Lett.* **95**, 146802 (2005).
19. Eremeev, S., Koroteev, Y. M. & Chulkov, E. V. Ternary thallium-based semimetal chalcogenides Tl-V-VI2 as a new class of three-dimensional topological insulators. *JETP Lett.* **91**, 594–598 (2010).
20. Singh, B., Lin, H., Prasad, R. & Bansil, A. Topological phase transition and quantum spin hall state in $TlBiS_2$. *J. Appl. Phys.* **116**, 033704 (2014).
21. Lee, K. *et al.* Discovery of a weak topological insulating state and van hove singularity in triclinic $RhBi_2$. *Nat. Commun.* **12**, 1–8 (2021).
22. Rusinov, I. P. *et al.* Mirror-symmetry protected non-trim surface state in the weak topological insulator Bi_2TeI. *Sci. Rep.* **6**, 1–7 (2016).
23. Majhi, K. *et al.* Emergence of a weak topological insulator from the Bi_xSe_y family. *Appl. Phys. Lett.* **110**, 162102 (2017).
24. Imura, K. I., Takane, Y. & Tanaka, A. Weak topological insulator with protected gapless helical states. *Phys. Rev. B* **84**, 035443 (2011).
25. Noguchi, R. *et al.* A weak topological insulator state in quasi-one-dimensional bismuth iodide. *Nature* **566**, 518–522 (2019).
26. Zhao, M., Dong, W. & Wang, A. Two-dimensional carbon topological insulators superior to graphene. *Sci. Rep.* **3**, 1–6 (2013).
27. Li, J. *et al.* Two-dimensional topological insulators with tunable band gaps: Single-layer HgTe and HgSe. *Sci. Rep.* **5**, 1–9 (2015).
28. Lohani, H. *et al.* Band structure of topological insulator $BiSbTe_{1.25}Se_{1.75}$. *Sci. Rep.* **7**, 1–10 (2017).
29. Chuang, F. C. *et al.* Prediction of large-gap two-dimensional topological insulators consisting of bilayers of group III elements with Bi. *Nano Lett.* **14**, 2505–2508 (2014).
30. Fu, B., Ge, Y., Su, W., Guo, W. & Liu, C.-C. A new kind of 2D topological insulators BiCN with a giant gap and its substrate effects. *Sci. Rep.* **6**, 1–7 (2016).
31. Das, T. *A Pedagogic Review on Designing Model Topological Insulators*. arXiv:1604.07546. (2016).
32. Zhou, L. *et al.* New family of quantum spin hall insulators in two-dimensional transition-metal halide with large nontrivial band gaps. *Nano Lett.* **15**, 7867–7872 (2015).
33. Hsieh, T. H. *et al.* Topological crystalline insulators in the SnTe material class. *Nat. Commun.* **3**, 1–7 (2012).
34. Kou, L., Ma, Y., Sun, Z., Heine, T. & Chen, C. Two-dimensional topological insulators: Progress and prospects. *J. Phys. Chem. Lett.* **8**, 1905–1919 (2017).
35. Edmonds, M. T. *et al.* Stability and surface reconstruction of topological insulator Bi_2Se_3 on exposure to atmosphere. *J. Phys. Chem. C* **118**, 20413–20419 (2014).
36. Yang, J. *et al.* Robust topological states in Bi_2Se_3 against surface oxidation. *J. Phys. Chem. C* **124**, 6253–6259 (2020).
37. Zhang, H. *et al.* Topological insulators in Bi_2Se_3, Bi_2Te_3 and Sb_2Te_3 with a single Dirac cone on the surface. *Nat. Phys.* **5**, 438–442 (2009).
38. Reid, T. K., Alpay, S. P., Balatsky, A. V. & Nayak, S. K. First-principles modeling of binary layered topological insulators: Structural optimization and exchange-correlation functionals. *Phys. Rev. B* **101**, 085140 (2020).
39. Brüne, C. *et al.* Quantum hall effect from the topological surface states of strained bulk HgTe. *Phys. Rev. Lett.* **106**, 126803 (2011).
40. Lin, H. *et al.* Adiabatic transformation as a search tool for new topological insulators: Distorted ternary Li_2AgSb-class semiconductors and related compounds. *Phys. Rev. B* **87**, 121202 (2013).
41. Feng, W., Xiao, D., Zhang, Y. & Yao, Y. Half-Heusler topological insulators: A first-principles study with the Tran-Blaha modified Becke-Johnson density functional. *Phys. Rev. B* **82**, 235121 (2010).
42. Xiao, D. *et al.* Half-heusler compounds as a new class of three-dimensional topological insulators. *Phys. Rev. Lett.* **105**, 096404 (2010).
43. Zhang, H.-J. *et al.* Topological insulators in ternary compounds with a honeycomb lattice. *Phys. Rev. Lett.* **106**, 156402 (2011).
44. Lee, S. *et al.* Single crystalline β-Ag_2Te nanowire as a new topological insulator. *Nano Lett.* **12**, 4194–4199 (2012).
45. Landolt, G. *et al.* Bulk and surface rashba splitting in single termination BiTeCl. *New J. Phys.* **15**, 085022 (2013).
46. Lin, H. *et al.* Single-Dirac-cone topological surface states in the $TlBiSe_2$ class of topological semiconductors. *Phys. Rev. Lett.* **105**, 036404 (2010).
47. Zhang, Q., Cheng, Y. & Schwingenschlögl, U. Emergence of topological and topological crystalline phases in $TlBiS_2$ and $TlSbS_2$. *Sci. Rep.* **5**, 1–7 (2015).
48. Singh, B., Lin, H., Prasad, R. & Bansil, A. Role of surface termination in realizing well-isolated topological surface states within the bulk band gap in $TlBiSe_2$ and $TlBiTe_2$. *Phys. Rev. B* **93**, 085113 (2016).
49. Eremeev, S. *et al.* Ab initio electronic structure of thallium-based topological insulators. *Phys. Rev. B* **83**, 205129 (2011).
50. Sato, T. *et al.* Direct evidence for the Dirac-cone topological surface states in the ternary chalcogenide $TlBiSe_2$. *Phys. Rev. Lett.* **105**, 136802 (2010).
51. Hsieh, D. *et al.* A topological Dirac insulator in a quantum spin hall phase. *Nature* **452**, 970–974 (2008).
52. Chen, Y. *et al.* Experimental realization of a three-dimensional topological insulator phase in ternary chalcogenide $TlBiSe_2$. *Phys. Rev. Lett.* **105**, 146801 (2010).
53. Ringel, Z., Kraus, Y. E. & Stern, A. Strong side of weak topological insulators. *Phys. Rev. B* **86**, 045102 (2012).
54. Hohenberg, P. & Kohn, W. Inhomogeneous electron gas. *Phys. Rev.* **136**, B864 (1964).
55. Kohn, W. & Sham, L. J. Self-consistent equations including exchange and correlation effects. *Phys. Rev.* **140**, A1133 (1965).
56. Kresse, G. & Joubert, D. From ultrasoft pseudopotentials to the projector augmented-wave method. *Phys. Rev. B* **59**, 1758 (1999).
57. Blöchl, P. E. Projector augmented-wave method. *Phys. Rev. B* **50**, 17953 (1994).
58. Kresse, G. & Furthmüller, J. Efficient iterative schemes for ab initio total-energy calculations using a plane-wave basis set. *Phys. Rev. B* **54**, 11169 (1996).
59. Perdew, J. P., Burke, K. & Ernzerhof, M. Generalized gradient approximation made simple. *Phys. Rev. Lett.* **77**, 3865 (1996).
60. Hedin, L. New method for calculating the one-particle green's function with application to the electron-gas problem. *Phys. Rev.* **139**, A796 (1965).

61. Togo, A., Oba, F. & Tanaka, I. First-principles calculations of the ferroelastic transition between rutile-type and $CaCl_2$-type SiO_2 at high pressures. *Phys. Rev. B* **78**, 134106 (2008).
62. Togo, A. & Tanaka, I. First principles phonon calculations in materials science. *Scr. Mater.* **108**, 1–5 (2015).
63. Giannozzi, P. *et al.* Quantum Espresso: A modular and open-source software project for quantum simulations of materials. *J. Phys.: Condens. Matter* **21**, 395502 (2009).
64. Mostofi, A. A. *et al.* Wannier90: A tool for obtaining maximally-localised wannier functions. *Comput. Phys. Commun.* **178**, 685–699 (2008).
65. Wu, Q., Zhang, S., Song, H.-F., Troyer, M. & Soluyanov, A. A. Wanniertools: An open-source software package for novel topological materials. *Comput. Phys. Commun.* **224**, 405–416 (2018).

Acknowledgements

A.P. acknowledges IIT Delhi for the junior research fellowship. P.B. acknowledges UGC, India, for the senior research fellowship [Grant no. 1392/(CSIR-UGC NET JUNE 2018)]. M.J. acknowledges CSIR, India, for the senior research fellowship [Grant No. 09/086(1344)/2018-EMR-I]. S.B. acknowledges financial support from SERB under a core research grant (Grant no. CRG/2019/000647) to set up his High Performance Computing (HPC) facility "Veena" at IIT Delhi for computational resources.

Author contributions

S.B. and A.P. conceived the project. S.B. supervised overall. A.P. performed all the calculations. A.P., P.B. and M.J. got involved in various discussion to analyze the data. All authors took part in finalizing the manuscript.

Competing interests

The authors declare no competing interests.

Additional information

Supplementary Information The online version contains supplementary material available at https://doi.org/10.1038/s41598-022-26445-y.

Correspondence and requests for materials should be addressed to A.P. or S.B.

Reprints and permissions information is available at www.nature.com/reprints.

Publisher's note Springer Nature remains neutral with regard to jurisdictional claims in published maps and institutional affiliations.